Ocean Dynamics (2015) 65:1335–1352
DOI 10.1007/s10236-015-0867-1

Impacts of mesoscale eddies in the South China Sea on biogeochemical cycles

Mingxian Guo[1,2] · Fei Chai[2] · Peng Xiu[3] · Shiyu Li[1] · Shivanesh Rao[2]

Received: 20 October 2014 / Accepted: 1 August 2015 / Published online: 13 August 2015

Abstract Biogeochemical cycles associated with mesoscale eddies in the South China Sea (SCS) were investigated. The study was based on a coupled physical–biogeochemical Pacific Ocean model (Regional Ocean Model System–Carbon, Silicate, and Nitrogen Ecosystem, ROMS-CoSiNE) simulation for the period from 1991 to 2008. A total of 568 mesoscale eddies with lifetime longer than 30 days were used in the analysis. Composite analysis revealed that the cyclonic eddies were associated with abundance of nutrients, phytoplankton, and zooplankton while the anticyclonic eddies depressed biogeochemical cycles, which are generally controlled by the eddy pumping mechanism. In addition, diatoms were dominant in phytoplankton species due to the abundance of silicate. Dipole structures of vertical fluxes with net upward motion in cyclonic eddies and net downward motion in anticyclonic eddies were revealed. During the lifetime of an eddy, the evolutions of physical, biological, and chemical structures were not linearly coupled at the eddy core where plankton grew, and composition of the community depended not only on the physical and chemical processes but also on the adjustments by the predator–prey relationship.

Keywords Mesoscale eddy · Biogeochemical cycles · South China Sea · Numerical model

Responsible Editor: Leo Oey

This article is part of the Topical Collection on the *6th International Workshop on Modeling the Ocean (IWMO) in Halifax, Nova Scotia, Canada 23-27 June 2014*

✉ Peng Xiu
pxiu@scsio.ac.cn

✉ Shiyu Li
eeslsy@mail.sysu.edu.cn

[1] Guangdong Provincial Key Laboratory of Environmental Pollution Control and Remediation Technology, School of Environmental Science and Engineering, Sun Yat-sen University, Guangzhou 510275, China

[2] School of Marine Sciences, University of Maine, Orono, ME 04469-5706, USA

[3] State Key Laboratory of Tropical Oceanography, South China Sea Institute of Oceanology, Chinese Academy of Sciences, Guangzhou 510301, China

1 Introduction

Mesoscale eddies are ubiquitous in world oceans. Comparing rotational speed with translational speed, most mesoscale eddies are found to be nonlinear in nature (Chelton et al. 2011b). Such nonlinearity implies that mesoscale eddies keep a coherent structure with fluid trapped in the eddy interior when propagating. Studies revealed that mesoscale eddies make great contributions to heat, salt, and mass transfers (Jayne and Marotzke 2002; Qiu and Chen 2005; Volkov et al. 2008; Dong et al. 2014; Zhang et al. 2014).

Nonlinear mesoscale eddies are also known to influence marine ecosystems. Biogeochemical cycles related to mesoscale eddy depend not only on the initial biogeochemical conditions of the water mass trapped inside the mesoscale eddy but also on nutrient supply. Several mechanisms have been proposed on how mesoscale eddies influence marine ecosystems: (1) During the formation of a mesoscale eddy, a cyclonic eddy shoals the isopycnal, which injects nutrients into the euphotic zone; an anticyclonic eddy deepens the isopycnal, which transports nutrients out of the euphotic zone in the eddy's interior. This mechanism is called eddy pumping (Siegel et al. 1999, 2011). In the Sargasso Sea, upwelling in cyclonic eddies was found to sustain an additional growth of

phytoplankton that cannot be fuelled by entrainment and diffusion-induced nutrient supply (McGillicuddy et al. 1998; McGillicuddy et al. 1999; Siegel et al. 1999). (2) Interaction of surface current and wind generates upwelling inside anticyclonic eddies and downwelling inside cyclonic eddies (Martin and Richards 2001; McGillicuddy et al. 2008; Gaube et al. 2013). These processes are called eddy-induced Ekman pumping (Siegel et al. 2011; Gaube et al. 2013). Upwelling generated by surface current and wind interaction was observed to cause phytoplankton blooms in anticyclonic eddies in the South Indian Ocean and in mode-water eddies in the subtropical Atlantic (McGillicuddy et al. 2007; McGillicuddy et al. 2008; Gaube et al. 2013). (3) Horizontal advection due to rotational velocities within an eddy results in meridional displacements of gradients of biological variables, such as nutrient and chlorophyll *a* (CHL). The advection of CHL due to horizontal rotation inside an eddy is called eddy advection (Siegel et al. 2008; Chelton et al. 2011a; Siegel et al. 2011). (4) Submesoscale processes are also reported to influence biogeochemical processes greatly (Lima et al. 2002). Due to instabilities, buoyancy loss or down-front wind, strong vertical flux or horizontal transport occurs in the euphotic zone in submesoscale processes (Thomas et al. 2013; Zhong and Bracco 2013). The intensity of horizontal and vertical fluxes can change the time that phytoplankton spend in the euphotic layer; so, submesoscale eddies can change not only the primary production and export but also the composition of the species (Lévy et al. 2012).

In the South China Sea (SCS), mesoscale eddies are ubiquitous (Wang et al. 2003). Approximately 33 mesoscale eddies appeared per year mainly in the northeast–southwest zone from the west of the Luzon Strait to the east of Vietnam, covering an area equivalent to 9.8 % of deep-sea area (water depth greater than 1000 m) in the SCS (Xiu et al. 2010). West of the Luzon Strait, due to fluctuations of the Kuroshio pathway and strong monsoon, mesoscale eddy kinetic energy is strong especially during the northeast monsoon (Chen et al. 2011; Nan et al. 2011). East of Vietnam, the dipole structure of the wind stress combined with complex topography produces high mesoscale eddy activities (Hwang and Chen 2000; Chen et al. 2010).

Impacts of mesoscale eddies on biogeochemical cycles and ecological systems in the SCS have been widely recognized. Previous studies have examined possible mechanisms based on which mesoscale eddies influence biogeochemical processes. A cyclonic eddy and two anticyclonic eddies were observed during cruises and studied by Chen et al. (2007) and Huang et al. (2010). Responses of ecological communities in both cyclonic and anticyclonic eddies were also studied using a model simulation (Xiu and Chai 2011). Enhanced primary productions in cyclonic eddies and deficient nutrients in anticyclonic eddies found by these studies suggested that eddy pumping may be a key factor in biogeochemical cycles. Composite analysis of sea surface CHL anomaly based on satellite data revealed that eddy-induced advection of CHL contributed to the propagation of CHL in the northern SCS where phytoplankton blooms were usually observed in winter (Wang et al. 2010; Liu et al. 2013). Other studies found that eddy-induced Ekman pumping could explain high CHL concentration in the interior of anticyclonic eddies in the SCS (Li et al. 2014). A ^{234}Th-based particle export study demonstrated that submesoscale processes combined with horizontal advection might enhance particle exports in anticyclonic eddy cores in the SCS (Zhou et al. 2013).

Since different physical processes were shown to influence the biogeochemical cycles of mesoscale eddies in the SCS, an analysis on general biogeochemical cycles of mesoscale eddies using a statistical method is necessary. However, previous studies about biogeochemical effects of mesoscale eddies in the SCS did not investigate general biogeochemical cycles in the eddy interior. Responses of biogeochemical processes inside eddies with the same polarity may be different if these eddies are controlled by different physical processes. For instance, eddy pumping in anticyclonic eddies transports nutrient-depleted water downward and suppresses the growth of phytoplankton, while eddy-induced Ekman pumping in anticyclonic eddies induces upward nutrient flux and contributes to phytoplankton growth (McGillicuddy et al. 1999; Ning et al. 2008; Gaube et al. 2013). In situ eddy observations revealed distributions of nutrients, phytoplankton community, and primary production in some eddies (Chen et al. 2007; Huang et al. 2010). But, these observations were based on limited sampling stations and therefore cannot reflect general biogeochemical cycles of mesoscale eddies in the SCS. Satellite-based ocean color data resolved mesoscale variability of sea surface CHL in time and space (Doney et al. 2003). However, studies based on satellite data cannot be used to investigate variability of nutrient distribution and evolution of biology communities at different water depths in the eddy interior. In fact, due to nutrient supply and predator–prey relationship, phytoplankton and zooplankton species were observed to change in time (Chai et al. 2002; Dugdale et al. 2002; Chai et al. 2007). Numerical simulations nowadays are capable of simulating physical and biological processes of mesoscale eddies over a long time period (Xiu et al. 2010, 2012; Xiu and Chai 2011). The goal of this study is to analyze general biogeochemical cycles of mesoscale eddies using a statistical method based on a coupled physical–biological ocean model simulation.

In this paper, we statistically analyze the biogeochemical cycles in the interior of mesoscale eddies in the SCS based on 17 years of output from a 3-D physical–biological coupled model simulation. We describe the data used to track eddies and the method used in the statistical analysis in Section 2. We focus on the influence of mesoscale eddies in sea surface CHL, biogeochemical cycles, and the evolution of ecological

communities, and discuss the mechanisms of mesoscale eddies on the biogeochemical cycles in Section 3. The findings of this study are summarized in Section 4.

2 Data and methods

2.1 Satellite data

In order to detect and track mesoscale eddies based on their sea surface height (SSH) signatures in satellite data, the merged sea level anomaly (SLA) field covering the study area from 5° N to 26° N and from 99° E to 120° E was obtained from the Archiving, Validation and Interpretation of Satellite Data in Oceanography (AVISO). The data is at 7-day interval on a grid of 1/4° by 1/4°. We use the data during a period from Jan. 1, 1998 to Dec. 31, 2007 in this study.

Daily sea surface CHL concentration from Jan. 1, 1998 to Dec. 31, 2007 was obtained from the National Aeronautic and Space Administration (NASA). The data was based on the measurements of Sea-Viewing Wide Field of View Sensor (SeaWiFS) that began its operation on Sep. 18, 1997 and stopped data collection on Dec. 11, 2010. The original grid resolution of the data is 9 km. Since the CHL concentration is derived from the ocean color, data at a location covered by clouds is not available. In order to reduce data gaps due to clouds, the daily CHL was $\log_{10}$-transformed and binned into a grid of 1/4° by 1/4°. After that, the time series of data at each grid point were low-pass filtered with a Loess window span of 30 days and averaged over 7-day interval. The regridded CHL data was then inverse-transformed using the inverse function of $\log_{10}$ (Gaube et al. 2013). The spatial resolutions of satellite SLA and CHL fields are now both 1/4° by 1/4°. In order to analyze these datasets using the same resolution of the model output, the satellite SLA and CHL were regridded again, to a grid with the resolution of 1/8° by 1/8°.

2.2 A coupled 3-D physical and biogeochemical model

In order to investigate the biogeochemical cycles in the interior of mesoscale eddies of the SCS, output from a Pacific basin physical–biogeochemical model simulation is analyzed in this study. The physical model is based on the Regional Ocean Model System (ROMS), which discretizes the primary equations over realistic topography and boundary using a stretched terrain-following coordinate (S coordinate system) in the vertical direction and orthogonal curvilinear coordinates on a staggered Arakawa C-grid in the horizontal direction (Song and Haidvogel 1994; Shchepetkin and McWilliams 2003, 2005). The model domain for the Pacific Ocean covers 45° S to 65° N and 99° E to 70° W. The resolution is 1/8° by 1/8° horizontally and 30 layers in the vertical. The model is first forced by climatological monthly heat and wind from the National Centers for Environmental Prediction/National Center for Atmospheric Research (NCEP/NCAR) reanalysis (Kalnay et al. 1996). The model is then run from 1991 to 2008 with daily heat fluxes, evaporation, and precipitation from the NCEP/NCAR reanalysis and daily sea surface winds from the NOAA multiple-satellite blended sea surface winds (Zhang et al. 2006). The output from both physical and biogeochemical models in the SCS (5° N to 26° N, 99° E to 120° E) is used to study the biogeochemical cycles inside mesoscale eddies. The vertical coordinate in the ROMS-Carbon, Silicate, and Nitrogen Ecosystem (CoSiNE) is also the S coordinate system. In our study, the vertical resolution between 0 and 200 m is uniform with a grid interval of 10 m. The model output from the ROMS-CoSiNE was interpolated into this vertical resolution before analysis.

The biogeochemical part of the model is based on the Carbon, Silicate, and Nitrogen Ecosystem (CoSiNE) model considering dissolved oxygen (O_2), carbon dioxide (CO_2), silicate (SiO_4), nitrate (NO_3), ammonium (NH_4), pico-phytoplankton (S1), diatom (S2), micro-zooplankton (ZZ1), meso-zooplankton (ZZ2), two detritus pools associated with ZZ1 and ZZ2, detrital nitrogen (DD), and detrital silicon (DDSi) (Chai et al. 2002; Dugdale et al. 2002). S1 represents phytoplankton in small size (<10 μm) that is grazed by Z1 (Chavez et al. 1991). S2 represents diatom (>10 μm) whose growth is limited by nitrogen and silicon bioavailability (Coale et al. 1996). The CoSiNE is initialized with nutrients from the World Ocean Atlas (WOA) 2001 and is run parallel with the physical model at every time step (Chai et al. 2007). The outputs of the model were averaged and saved every 3 days.

The model results have been used to study physical–biogeochemical processes in the Pacific Ocean. An oceanic carbon cycle study in the tropical–subtropical Pacific Ocean using a coarse grid revealed that the model can simulate the distribution of SST and the temporal variation of dissolve inorganic carbon (Fujii et al. 2009). The model output was used to study the dynamics of physical–biological processes in coastal and offshore area of the central California current system (Guo et al. 2014). The model was also used in studying the biogeochemical processes and eddy activities in the SCS. An eddy census study revealed that the model is capable of simulating the eddy distribution and inter-annual variability of eddy genesis number and eddy kinetic energy in the SCS (Xiu et al. 2010). The model was also used to study the temporal biogeochemical variance in cyclonic and anticyclonic eddies of the SCS (Xiu and Chai 2011). A study of biological responses to the jet off Vietnam revealed that the model can simulate the physical and biogeochemical processes east of Vietnam (Chen et al. 2014). Studies on biological productivity showed that the model reproduced the vertical distribution and annual variability of nutrients, CHL, and primary production (Chai et al. 2009; Liu and Chai 2009; Xiu et al. 2012). All

these studies demonstrated that the model simulation can be used to study the biogeochemical processes of mesoscale eddies in the SCS.

In summer, the area off the northwest of Luzon Island is mainly occupied by anticyclonic eddies, and concentrations of CHL are observed to be low (Yuan et al. 2007). Eddy pairs occur east of Vietnam at this season as well (Chen et al. 2010). Due to upwelling and offshore transport by a jet, enhanced concentrations of CHL were frequently observed east of Vietnam (Zhao and Tang 2007; Chen et al. 2014). In order to validate the model, we compared the spatial distribution of climatological SLA and CHL in August between model output and satellite data (Fig. 1). Signals of the anticyclonic eddies off the northwest of Luzon Island and of Vietnam dipole east of Vietnam can be seen in both satellite and model results (Fig. 1a, b). Comparing with the satellite result, the modeled SLA off the northwest of Luzon Island is weaker while that east of Vietnam is stronger. For CHL, although the simulated CHL in oligotrophic area is lower than the satellite results, the model is capable of reproducing phytoplankton blooms east of Vietnam and low CHL concentrations off the northeast of Luzon Island (Fig. 1c, d).

We also examined the seasonal and inter-annual variations of model simulation. The time series of SLA averaged over the deep area where water depth is greater than 1000 m show that the model simulation agrees well with the satellite data in terms of seasonal and inter-annual variations, with a correlation coefficient of 0.80 (Fig. 2). The high correlation can be clearly seen in the comparison of sea surface CHL averaged over deep area as well (Fig. 3). Although the modeled CHL tends to overestimate the seasonal variability, the correlation between model and satellite is significantly high with a correlation coefficient of 0.87. The discrepancy is probably due to that one set of model parameters being insufficient to cover the entire SCS including diverse biological provinces.

2.3 Eddy tracking

The Okubo–Weiss method is widely used to detect mesoscale eddies (Okubo 1970; Weiss 1991; Frenger et al. 2013). However, its criterion based on strain and vorticity of the eddy to identify eddy core has been found to underestimate eddy-occupied area (Basdevant and Philipovitch 1994). In this study, the procedure based on the Okubo–Weiss with an improvement in determining eddy core was used to identify and track mesoscale eddies. Detail of this procedure can be found in Xiu et al. (2010). Mesoscale eddies were identified and tracked from the SLA field of both satellite data and model output. Since the SLA is not reliable in shallow waters, we only considered SLA in the area whose water depth is greater than 1000 m. An individual eddy identified at each time step is referred as eddy realization. In the coordinate grid, the grid points in the interior of each eddy realization are marked as eddy points. The position of eddy realization centroid is specified by averaging the locations of all eddy points belonging to this eddy in the zonal and meridional coordinate, respectively.

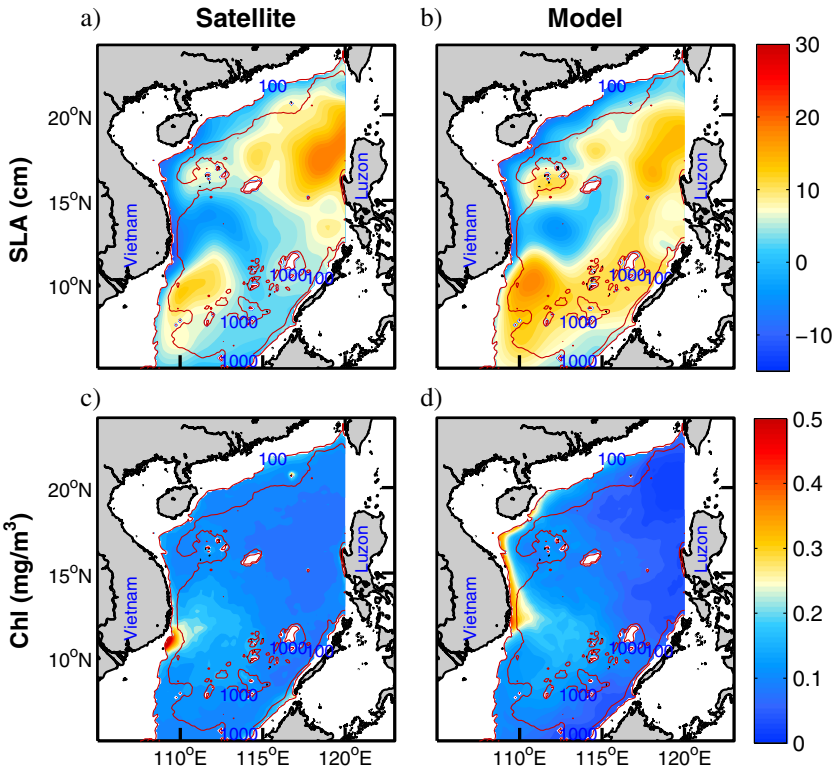

Fig. 1 Comparison of climatological SLA (*first row*) and CHL (*second row*) for August in area of the SCS where water depth is greater than 100 m between model output (*first column*) and satellite data (*second column*). *Contour lines* overlaid on each panel are 100- and 1000-m isobaths

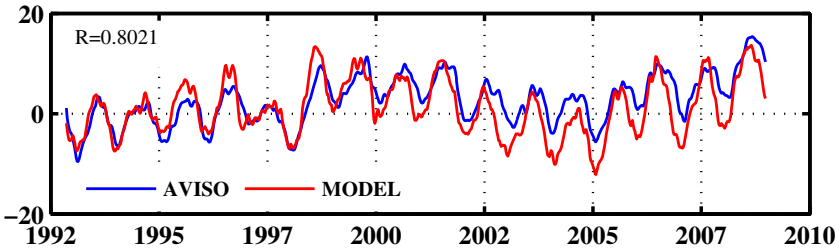

Fig. 2 Time series of SLA averaged over area of the SCS whose water depth is greater than 1000 m based on model output (in *red*) and AVISO data (in *blue*) from Nov. 11, 1992 to Dec. 24, 2008

Zonal scale (L_Z) and meridional scale (L_M) of each eddy realization are defined as the difference of maximum and minimum coordinates of eddy points belonging to this eddy realization in the zonal and meridional coordinate, respectively. Eddy radius R is then defined as half of the averaged L_Z and L_M. In the procedure, eddy realizations with radius less than 45 km are all discarded. After identifying all possible eddy realizations, eddy trajectories are specified using a connectivity algorithm described in Xiu et al. (2010) so that eddy lifetime can be calculated. In our study, eddies with lifetime less than 28 days in satellite SLA field or less than 30 days in model SLA are also discarded.

2.4 Making composite

To investigate general biogeochemical cycles of mesoscale eddies in the SCS, the mesoscale eddies tracked in both satellite and model SLA fields are first normalized in space so that they can be used in composite analysis (Chelton et al. 2011a; Gaube et al. 2013). The radii of these eddies range from 45 km to more than 200 km (Fig. 4), with an averaged radius of 89.22 km in the model and 86.35 km in the satellite data. In order to normalize the eddies in space, snapshots in weekly or 3-day time step along the eddy trajectories were extracted following the steps below:

1. At each time step along the trajectory of an eddy, taking the eddy realization centroid as the coordinate origin, a rectangular area is determined from $-2R$ to $2R$ in both zonal and meridional directions, where R is the radius. The eddy realization area is defined as a circular area that is based on the coordinate origin and the radius. So, this rectangular area includes the eddy and its surrounding water area.
2. The spatial scale ($-2R$ to $2R$) in both zonal and meridional directions is then projected into (-2 to 2) so that the rectangular area is normalized as a box that has a range of (-2 to 2) in both zonal and meridional directions.
3. The rectangular area obtained in step 2 is then interpolated into a uniform grid that ranges from -2 to 2 and has a grid size of 0.1 in both x and y directions.
4. Steps 1–3 are conducted for every time step along the eddy trajectory, and snapshots at each time step are extracted for this eddy track.
5. Since the snapshots of all eddies have the same uniform grid, they can be composited to obtain the averaged physical and biogeochemical variables.

2.5 Time normalizing

By analyzing the variation of plankton (S1, S2, ZZ1, and ZZ2) and detritus (DD and DDSi) biomass during eddy lifetime, evolutions of biological community in the interior of mesoscale eddies can be investigated. As Fig. 4 (right) shows, eddy lifetime L ranges from 30 to 162 days. If we want to analyze the general evolution of biological communities among several eddies, each eddy lifetime should be normalized first so that time series of plankton and detritus biomass following eddy lifetime can be constructed from different eddies. The normalization procedure is as follows:

1. At each grid point, integrated biomasses of plankton and detritus from 0 to 100 m are calculated. For each eddy realization, integrated biomass is averaged at each grid

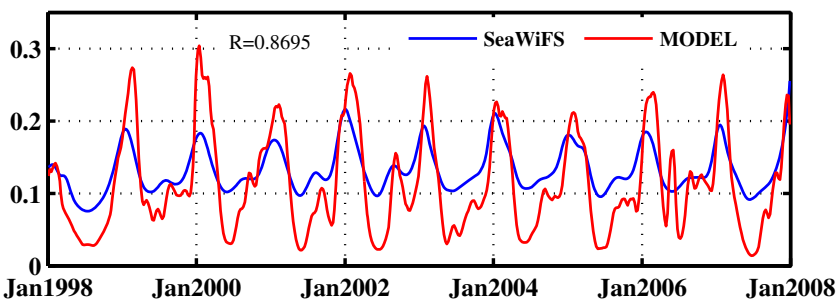

Fig. 3 Time series of sea surface CHL averaged over area of the SCS where water depth is greater than 1000 m based on model output (in *red*) and SeaWiFS data (in *blue*) from Jan. 1, 1998 to Dec. 31, 2007

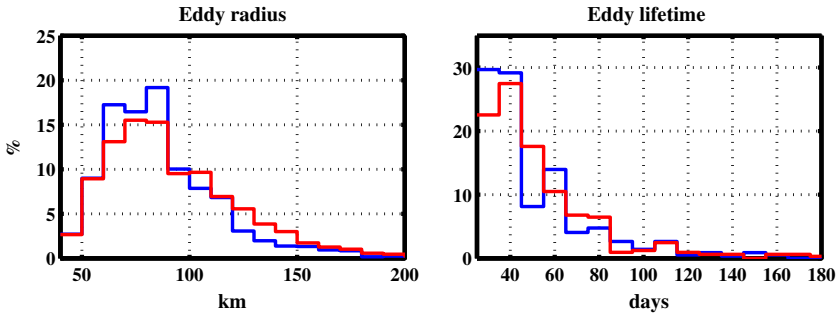

Fig. 4 Histogram of radius (*left*) and lifetime (*right*) for eddies tracked from 1998 to 2007. *Red lines* represent model results and *blue lines* represent satellite results

point that is in the interior of the eddy realization. Following eddy lifetime, the time series of integrated biomass for each eddy are obtained.

2. The time grid for the time series of integrated biomass of each eddy ranges from 0 to L with an interval of 3 days. The value at each time step of the time grid is divided by L so that the normalized time grid is from 0 to 1.
3. A uniform time grid ranging from 0 to 1 with a time interval of 0.05 is then created. Integrated biomass of plankton and detritus as a function of time grid described in step 2 is interpolated into this uniform time grid.

Steps 1–3 were performed for all the eddies used in this study to analyze the evolution of biological communities. After that, time series of composite averaged biomass are constructed from these eddies.

3 Results

3.1 Satellite and model comparison

Using the procedure described in Section 2.3, 329 cyclonic eddies with 5678 snapshots and 239 anticyclonic eddies with 4586 snapshots were tracked in the model SLA field over 18 years. Similarly, 1237 snapshots from 173 cyclonic eddies and 1159 snapshots from 146 anticyclonic eddies were obtained in the satellite SLA field from 1998 to 2007. On average, the number of eddies was 31.6/year in the model SLA field and was 31.9/year in the satellite SLA field; they are close to 32.9/year in Xiu et al. (2010).

In order to assess whether the model is able to simulate eddies in the SCS, comparison of eddy characteristics between model and satellite data is done. Histograms of eddy lifetime and radius over 1998–2007 for both the model and satellite data are shown in Fig. 4. The model is capable of reproducing the most frequently occurred eddy scales, which range from 60 to 80 km (see Fig. 4a). The mean radius in the model is 89.22 km, which is greater than 86.35 km in the satellite data, owing to an underestimation of distribution for the eddies with radius in the range of 60 km$<R<$80 km and to an overestimation of distribution for eddies with radius in the range of 120 km$<R<$150 km. The average eddy lifetime in the model is 54.5 days, which is close to 50.2 days of the satellite data. To evaluate eddy spatial distribution, the number of eddy realization centroids in each 1°×1° bin over the period of 1998–2007 is counted, and their ratio to total eddy centroids counted over the entire SCS is shown in Fig. 5. Comparing with the satellite result, the model is capable of simulating the spatial distribution of eddy centroids. High frequency of eddy centroid occurrence west of the Luzon Strait and the area off southwest of Luzon Island is reproduced in the model. The high eddy activity to the west of the Luzon Strait is due to a combination of wind (Yang and Liu 2003), eddy shedding from the Kuroshio (Jia and Liu 2004), and instability of the Kuroshio path (Nan et al. 2011). The model, however, overestimates the eddy centroid occurrence along the northern continental slope. The model also underestimates the distribution of eddy centroids in the area off northwest of Luzon Island and off Vietnam. A previous study revealed that the interaction between wind-driven coastal currents and shelf topography in the nearshore waters plays a crucial role in eddy generation (Gan and Qu 2008). The underestimation of eddy activities is likely due to topography smoothing in our model setup.

In summary, the average numbers of mesoscale eddies tracked in both model and satellite fields are found to be close to those in previous studies (Wang et al. 2003; Xiu et al. 2010; Chen et al. 2011). Distribution of eddy centroid, and censuses of eddy lifetime and radius in the model are also consistent with the satellite results. We conclude that the ROMS-CoSiNE Pacific model is able to simulate the activity of mesoscale eddies in the SCS.

In the SCS, eddy advection, eddy pumping, and eddy-induced Ekman pumping greatly influence distribution of sea surface CHL concentration based on satellite observations (Liu et al. 2013; Chen et al. 2014; Li et al. 2014). Sea surface CHL in the eddy interior can be different among eddies if biogeochemical cycles are controlled by different physical processes. In order to study the main contribution of mesoscale eddies on CHL, composite averages of SLA and CHL

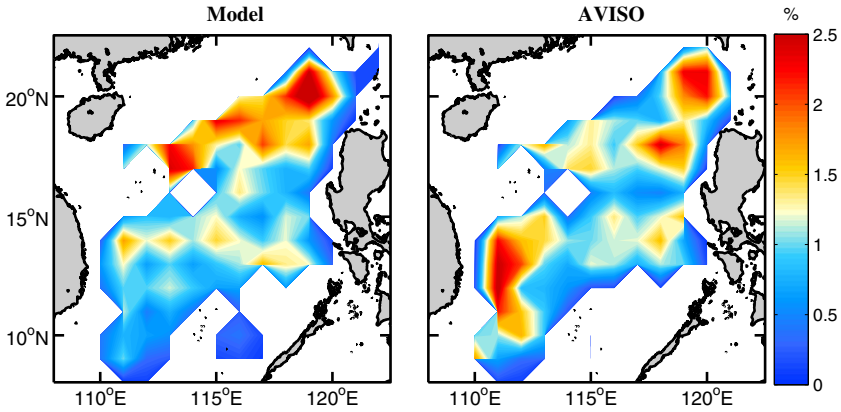

Fig. 5 Spatial distribution of eddy realization centroid for eddies tracked in (*left*) model and (*right*) satellite SLA fields during 1998–2007

are constructed from thousands of normalized eddy snapshots described in Section 2.3.

Composite averages of SLA are shown in Fig. 6. The shape of composite SLA is centrosymmetric despite that the zonal scale L_Z and meridional scale L_M for each eddy realization are usually not the same. Here, eddy amplitude is defined as the difference of SLA in the centroid and edge of the constructed eddy. In the satellite data, the amplitude for cyclonic eddies is 7.4 cm and that for anticyclonic eddies is 7.9 cm. The amplitudes from the satellite data are close to the global mean amplitude of 8 cm (Chelton et al. 2011b). In the model results, the amplitude is 10.6 cm for cyclonic eddies and 10.9 cm for anticyclonic eddies. So, our model overestimates the amplitudes of eddies in the SCS.

Composite averages of CHL are shown in Fig. 7. In the satellite results, background northwest–southeastward CHL gradients with maximum CHL of 0.18 mg/m^3 at the northeast corner are shown clearly in panels a and b. Although the

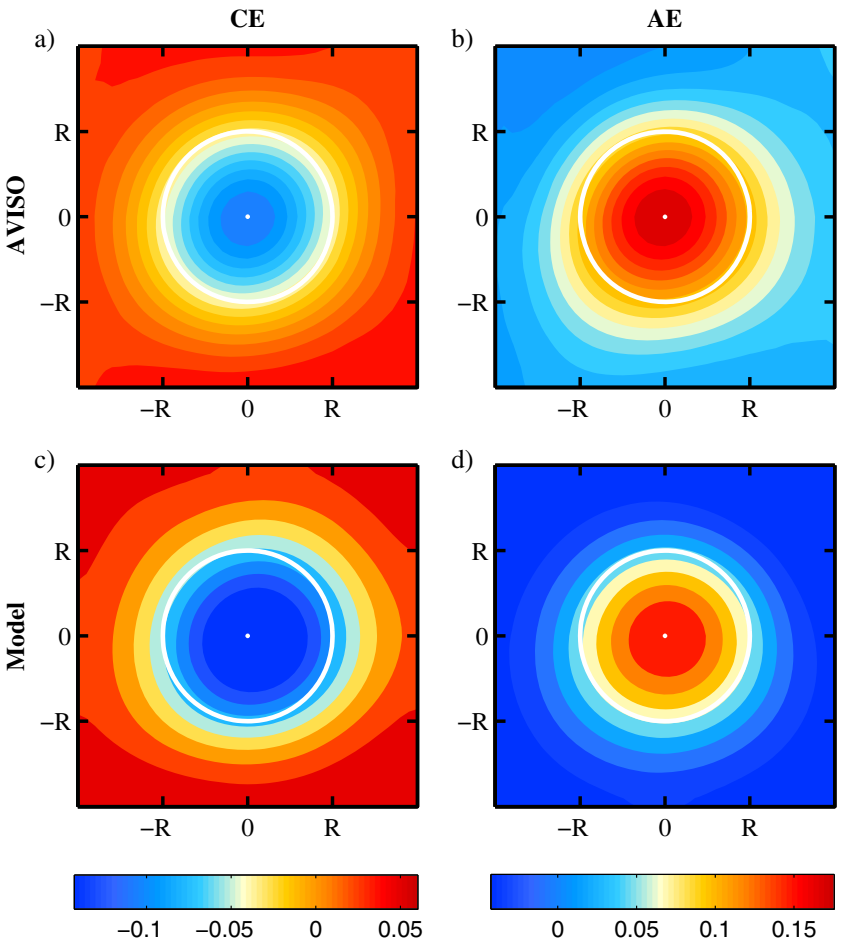

Fig. 6 Composite averages of (*first row*) AVISO- and (*second row*) model-based SLA for (*first column*) cyclonic eddies and (*second column*) anticyclonic eddies tracked from 1998 to 2007. *White lines* are circles with distance of *R* from the center (*white point*) of each panel

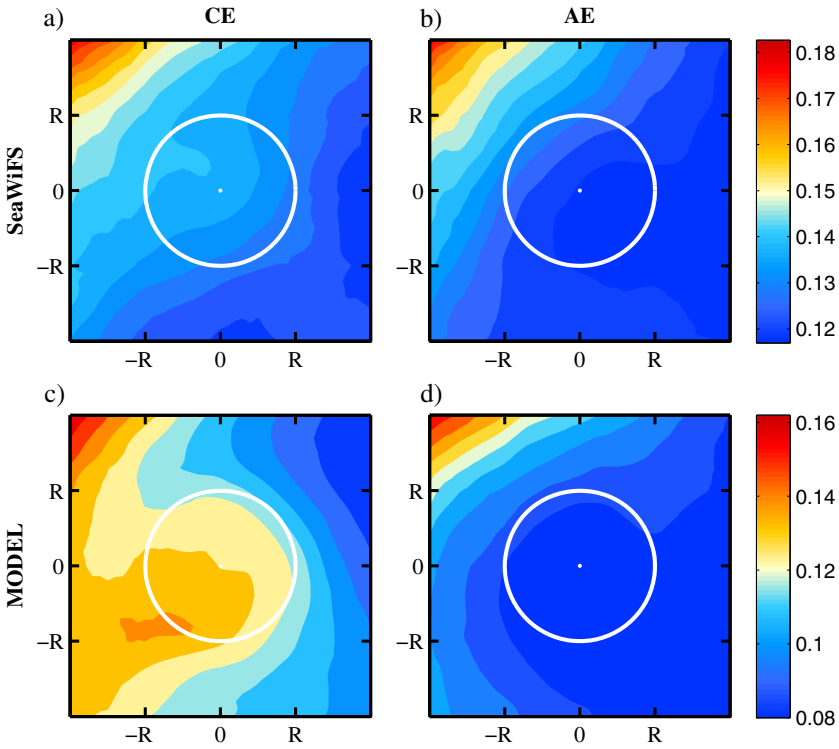

Fig. 7 Composite averages of (*first row*) SeaWiFS- and (*second row*) model-based CHL for (*first column*) cyclonic and (*second column*) anticyclonic eddies tracked from 1998 to 2007. *White lines* are circles with distance of *R* from the center (*white point*) of each panel

mesoscale eddies were identified in the deep-sea area (water depth >1000 m), snapshots for each eddy realization have double length of eddy radius in the zonal and meridional directions. Therefore, high CHL values over the northern continental shelf and the coastal area off Vietnam appear at the northwest corner of these panels. The average CHL at eddy-occupied area is 0.14 mg/m^3 for the cyclonic eddies and 0.12 mg/m^3 for the anticyclonic eddies. Comparing CHL values at eddy cores with background CHL at the northeast edge, high CHL is associated with the cyclonic eddies while low CHL is associated with the anticyclonic eddies. A meander of CHL distribution around the cyclonic eddy core indicates eddy advection of CHL.

The background CHL gradients in the model are shown in panels c and d, with the maximum value of 0.16 mg/m^3. Underestimation of CHL at the northwest corner is partly because our model does not consider river input and partly because the SeaWiFS data in the coastal area is unreliable (Liu et al. 2002). High CHL at the cyclonic eddy core and low CHL at the anticyclonic eddy core can be seen in the model results as well. The high CHL at the cyclonic core is consistent with cruise observations (see Table 1). The average CHL at the core is 0.14 mg/m^3 for the cyclonic eddies and 0.076 mg/m^3 for the anticyclonic eddies. High CHL at the west edge of model-based cyclonic eddy core indicates eddy advection of CHL more clearly.

An interpretation for high CHL at the cyclonic eddy core and low CHL at the anticyclonic eddy core is that eddy pumping plays an important role on surface CHL distribution of eddies (McGillicuddy et al. 1998, 1999; Siegel et al. 1999). This interpretation has been tested statistically in biooptical footprint studies (Chelton et al. 2011a; Siegel et al. 2011; Liu et al. 2013). Horizontal advection of CHL by eddy rotation was investigated in previous studies (Chelton et al. 2011a; Siegel et al. 2011). In our study, high CHL at the west edge of cyclonic-eddy-occupied area suggests that anticlockwise rotation in the west part of an eddy advects high CHL from northwest to west. A previous study showed that larger amplitude results in higher rotational velocity (Chelton et al. 2011a). Owing to overestimation of eddy amplitude, the advection of CHL in the model results is stronger than that in the satellite results.

3.2 Biogeochemical cycles

To investigate the main influence of mesoscale eddies in the SCS on biogeochemical cycles, composite averages of nutrients, phytoplankton, and zooplankton were constructed from the 329 cyclonic eddies with 5678 snapshots and 239 anticyclonic eddies with 4586 snapshots detected from 1991 to 2008.

3.2.1 Nutrients

Composite averages of nitrate and silicate concentrations averaged in the top 50 m for the cyclonic eddies are shown in Fig. 8a, b. Black contours represent the composite SLA. Comparing with the surrounding waters, concentrations of

Table 1 Comparison of near-sea-surface physical and biogeochemical variables between model composite and Chen's sampling stations in Chen et al. (2007)

Variables	Chen's sampling observation		Model composite	
	Eddy station	SCS stations	Center	Periphery
Temperature (°C)	25.8	26.9	23.2	24.6
Salinity (psu)	34.49	34.36	34.48	34.38
NO_3+NO_2 (mmol N m^{-3})	0.107	0.014	0.82	0.59
SiO_2 (mmol Si m^{-3})	2.43	1.89	3.11	2.82
CHL (mg m^{-3})	0.4	0.13	0.12	0.1
Picophytoplankton	216.89 (10^6 L^{-1})	183.9 (10^6 L^{-1})	0.052 mmol N/m^3	0.045 mmol N/m^3
Diatoms	2837 (cells L^{-1})	84 (cells L^{-1})	0.116 mmol N/m^3	0.106 mmol N/m^3

SCS South China Sea, *CHL* chlorophyll *a*

nutrients are high in eddy-occupied areas. Statistical result suggests that cyclonic eddies enhance nutrients in the interior of cyclonic eddies. The maximum concentrations are found to be in the centroid, with values of 0.82 mmol N/m^3 for nitrate and 3.11 mmol Si/m^3 for silicate. The abundance of nutrients in the interior of a cyclonic eddy is consistent with a study using cruise data in the SCS (see Table 1) (Chen et al. 2007). The average concentration of silicate in the eddy interior was about four times as that of nitrate, indicating that the fluid inside the cyclonic eddy was silicate dominant. The phenomenon that concentration of silicate was higher than that of nitrate was found in a previous study using cruise observations (see Table 1) (Chen et al. 2007). Distribution of nutrients in the background reflects a basin-scale northwest–southeast gradient since nutrients in the northern continental shelf and off Vietnam are usually higher than those in the open ocean area.

In the case of the anticyclonic eddies, the background gradient distribution of nutrients averaged in the top 50 m was

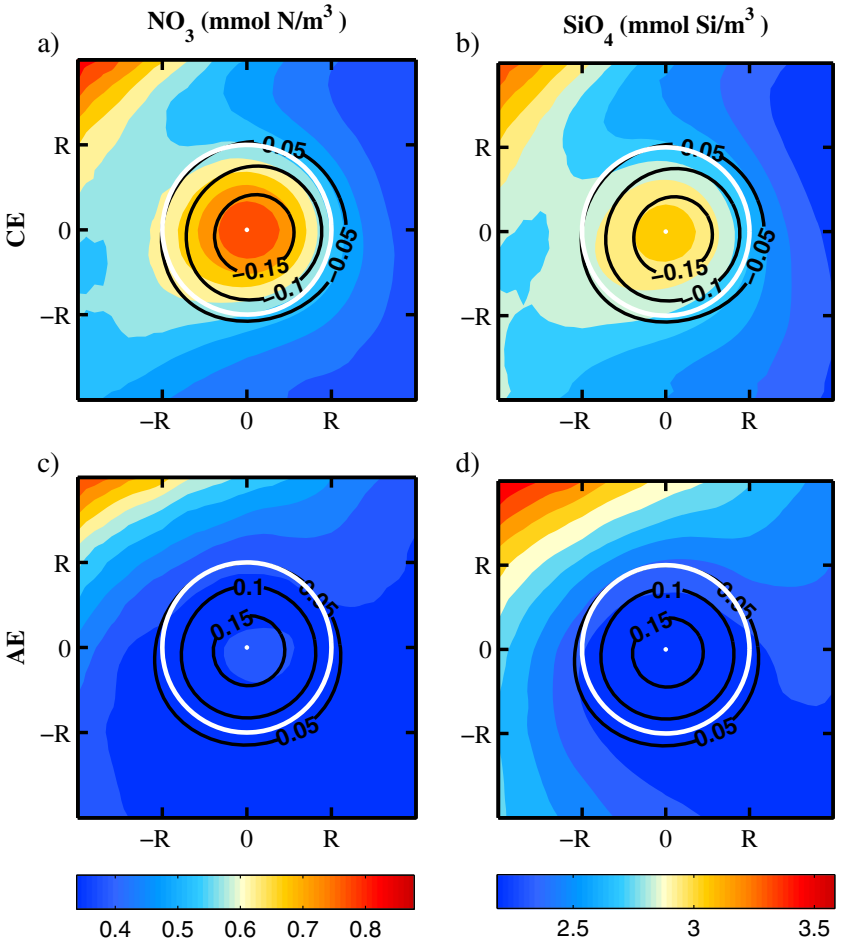

Fig. 8 Composite averages of (*first column*) NO_3 and (*second column*) SiO_4 in upper 50-m average result overlaid with contours of sea level anomaly for (*first row*) cyclonic eddies and (*second row*) anticyclonic eddies. *White lines* are circles with distance of *R* from the center (*white point*) of each panel

also southeastward disregarding eddy-occupied areas (Fig. 8c for nitrate and Fig. 8d for silicate). Although the concentrations of silicate and nitrate were both low at the constructed eddy core, their distributions were different. For nitrate, the concentration decreased from 0.39 mmol N/m^3 at the centroid to 0.37 mmol N/m^3 at the edge. However, considering the entire eddy core, nitrate concentration is still significantly lower than that in surrounding waters. For silicate, the lowest concentration was at the eddy centroid.

3.2.2 Phytoplankton

In this study, pico-phytoplankton (S1) and diatoms (S2) are considered. In our model, pico-phytoplankton feeds on nitrate and diatoms using both nitrate and silicate (Chai et al. 2002; Dugdale et al. 2002). In the cyclonic eddies, as the nutrients in the core are found to be more abundant compared to those in the periphery water from the composites (Fig. 8), S1 and S2 in the eddy core are expected to be higher than in the surrounding water. These results can be found from the composite of phytoplankton concentration averaged in the top 50 m and biomass integrated in the top 100 m. Figure 9a, b shows that the concentrations of S1 and S2 in the eddy center are 0.052 and 0.116 mmol N/m^3 and decrease to 0.045 and 0.106 mmol N/m^3 at the edge, respectively. In cruise data, the concentrations of S1 and S2 were abundant in the cold eddy comparing with the surrounding water (see Table 1) (Chen et al. 2007). In the model result, depth-integrated biomasses of S1 and S2 are higher in the core than those in the periphery (Fig. 10). Biomass of S2 decreased from 13.27 mmol N/m^2 in the centroid to 11.73 mmol N/m^2 at the edge. In S1 composite, the maximum biomass was a bit off the eddy center, with a value of 3.51 mmol N/m^2. Because of the abundance of silicate (Fig. 8a, b), the ratio of S2 to total phytoplankton integrated in the euphotic zone was up to 70 % in the eddy core (right panel in Fig. 10). Our study shows that dominance of diatoms existed in the interior of mesoscale eddies. Analogous abundance of diatoms in cold eddies was observed in subtropical North Atlantic and Pacific. In their research, Bibby and Moore (2010) found that the relative abundance of silicate over nitrate determines the abundance of diatoms in mesoscale eddies.

In the anticyclonic eddies, the composites of S1 (Fig. 9c) and S2 (Fig. 9d) in the top 50 m show that the average concentrations of S1 and S2 in the core are 0.017 and 0.076 mmol N/m^3. In the periphery area, the average

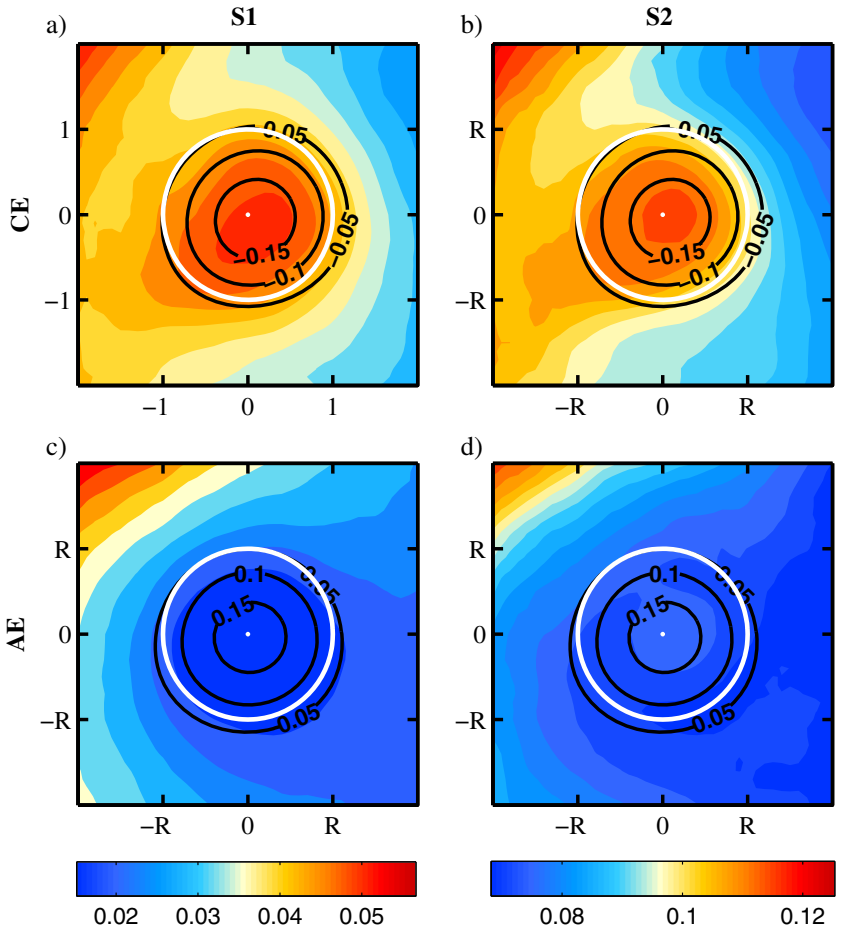

Fig. 9 Composite averages of (*first column*) S1 and (*second column*) S2 in upper 50-m average result overlaid with contours of sea level anomaly for (*first row*) cyclonic eddies and (*second row*) anticyclonic eddies. *White lines* are circles with distance of *R* from the center (*white point*) of each panel. Unit: mmol N/m^3

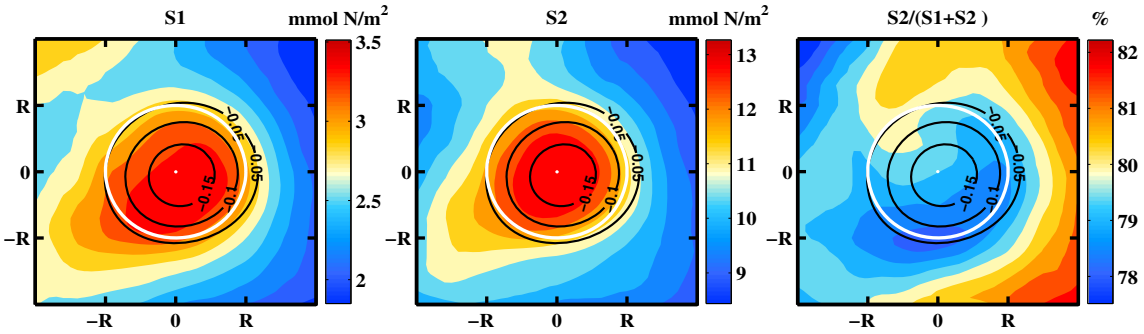

Fig. 10 Composite averages of (*left*) S1 and (*middle*) S2 in 100-m integrated result and (*right*) the corresponding biomass ratio of S2 to the total phytoplankton overlaid with contours of sea level anomaly for cyclonic eddies. *White lines* are circles with distance of *R* from the center (*white point*) of each panel

concentrations of S1 and S2 are 0.02 and 0.08 mmol N/m^3. The concentrations of phytoplankton are notably lower in the eddy core than those in the periphery. This result is consistent with the model study of Xiu and Chai (2011). The concentration of diatoms increased from 0.074 mmol N/m^3 at the edge to 0.078 mmol N/m^3 in the eddy center. This indicates that some anticyclonic eddies might have induced upward nutrient flux and caused increase of diatoms, but note that the increase was only about 5 % from the edge to the core. Actually, given the entire eddy core, diatom concentration was significantly lower than that in surrounding waters.

3.2.3 Zooplankton

In the marine ecosystem, phytoplankton is a food source for zooplankton. The growth of ZZ1 depends on S1, and that of ZZ2 depends on S2 and ZZ1 (Chai et al. 2002; Dugdale et al. 2002). In order to study the influence of mesoscale eddies on zooplankton, the composites of ZZ1 and ZZ2 averaged in the top 50 m are constructed for both cyclonic and anticyclonic eddies (Fig. 11). Since the concentrations of S1 and S2 were high in the cyclonic cores, the concentrations of ZZ1 and ZZ2 were larger in the cyclonic eddy interior than in the periphery. The concentrations of ZZ1 and ZZ2 increased gradually from the edge with the values of 0.015 and 0.033 mmol N/m^3 toward the eddy center with average concentrations of 0.018 and 0.043 mmol N/m^3, respectively. In order to confirm the abundance of zooplankton in the cyclonic eddies, the biomass composites of ZZ1 and ZZ2 integrated in the euphotic zone are also constructed (see left and middle panels of Fig. 12), which show that the biomasses of ZZ1 and ZZ2 varied from 0.930 and 2.905 mmol N/m^2 to 3.597 and 1.051 mmol N/m^2, respectively.

In the anticyclonic eddies, the composite averages (Fig. 11c, d) show that the concentrations of ZZ1 (Fig. 11c) and ZZ2 (Fig. 11d) in the top 50 m were all low in the eddy-occupied area compared with those in the background. The concentrations of ZZ1 and ZZ2 decreased slightly from the edge with values of 0.004 and 0.011 mmol N/m^3 to the center with values of 0.002 and 0.008 mmol N/m^3, respectively.

3.2.4 Horizontal currents, vertical nutrient flux, and net primary production

To understand how mesoscale eddies induce upward nutrient flux to the euphotic zone and what causes the distribution of nutrients and plankton, composite averages of horizontal current velocity averaged in the top 50 m, the nutrient flux (defined as the sum of silicate and nitrate concentrations multiplying the vertical velocity) at the bottom of euphotic zone, and net primary production at 50 m are constructed from the mesoscale eddies tracked in the model SLA. Figure 13a, c shows the composite averages of vertical nutrient fluxes (colors) and horizontal currents (arrows) for the cyclonic eddies and anticyclonic eddies, respectively. Both vertical nutrient fluxes had a dipole structure. Strong upwelling and downwelling occurred at the edge of the mesoscale eddies. In the cyclonic eddy composite, the upward flux core with a maximum flux of 2.3E-03 mmol N/m^2/s was located at the northern edge, and the downward flux core with a maximum value of 1.9E-03 mmol N/m^2/s was located in the southwestern edge. The average vertical nutrient flux was 5.2E-04 mmol N/m^2/s, indicating that the vertical nutrient flux in the cyclonic eddies was upward. In the anticyclonic eddy results, the upward and downward motions were at the southeastern and northwestern edges, with maximum fluxes of 8.8E-04 and 1.4E-03 mmol N/m^2/s, respectively. The net flux in the eddy interior was −1.0E-04 mmol N/m^2/s. In the composites, the constructed horizontal velocities are also shown. The composites of net primary production are shown in the second column of Fig. 13. The spatial distributions of net primary production were homogenous in both cyclonic and anticyclonic eddies. The value increased from 0.032 mmol N/m^3/day at the edge to 0.039 mmol N/m^3/day at the centroid of the cyclonic eddies and decreased from 0.015 mmol N/m^3/day at the edge to 0.014 mmol N/m^3/day at the centroid of the anticyclonic eddies.

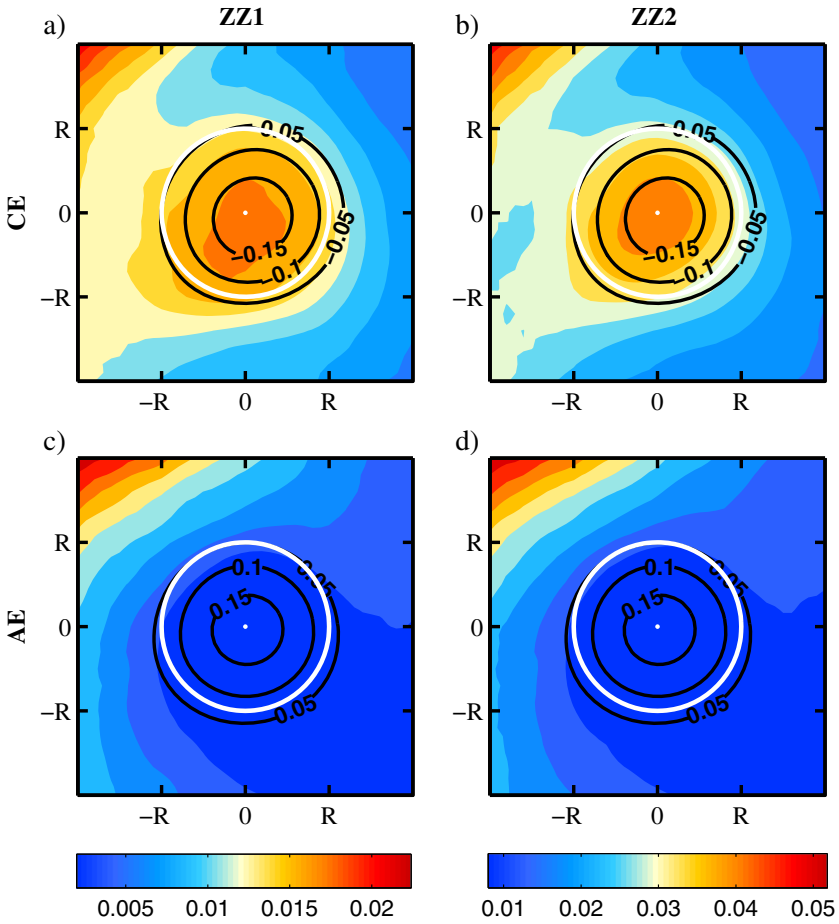

Fig. 11 Composite averages of (*first column*) ZZ1 and (*second column*) ZZ2 in upper 50-m average result overlaid with contours of sea level anomaly for (*first row*) cyclonic eddies and (*second row*) anticyclonic eddies. *White lines* are circles with distance of *R* from the center (*white point*) of each panel. Unit: mmol N/m^3

3.2.5 Discussion of biogeochemical cycles

The abundance of nutrients, phytoplankton, and zooplankton in the cold eddies of the SCS was investigated using cruise observations (Chen et al. 2007) and model output (Xiu and Chai 2011). These studies were based on individual sampling analysis. In our research, the statistical analysis confirmed that the cyclonic eddies enhanced nutrients and stimulated the growth of phytoplankton and zooplankton. In the case of anticyclonic eddies, our results showed that the anticyclonic eddies decreased nutrients and suppressed the growth of phytoplankton and zooplankton. This is consistent with Huang et al. (2010) using cruise data and with Xiu and Chai (2011) using model output. The dominance of diatoms is coincident with a phytoplankton structure study in the SCS (Ma et al. 2013). It was proposed that the community structure in mesoscale eddies is controlled by the ratio of silicate to nitrate (Bibby and Moore 2010). This explains the dominance of diatoms in the mesoscale eddies in the SCS. The cores with weak upward motion in the anticyclonic eddies also made it

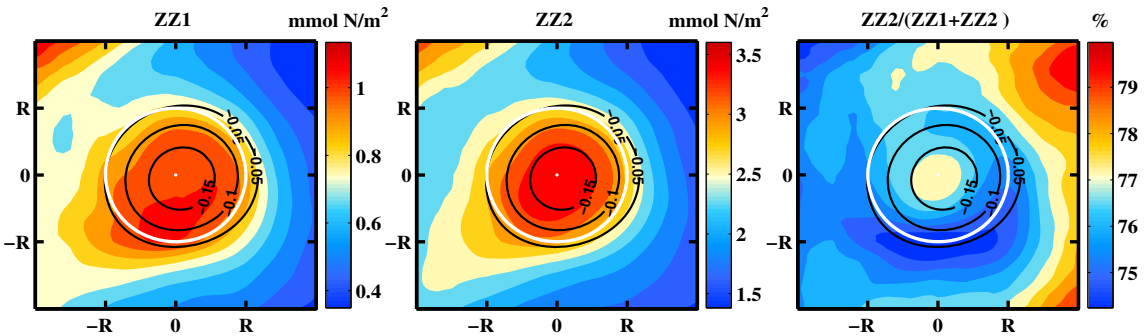

Fig. 12 Composite averages of (*left*) ZZ1 and (*middle*) ZZ2 in 100-m integrated result and (*right*) the corresponding biomass ratio of ZZ2 to the total zooplankton overlaid with contours of sea level anomaly for cyclonic eddies. *White lines* are circles with distance of *R* from the center (*white point*) of each panel

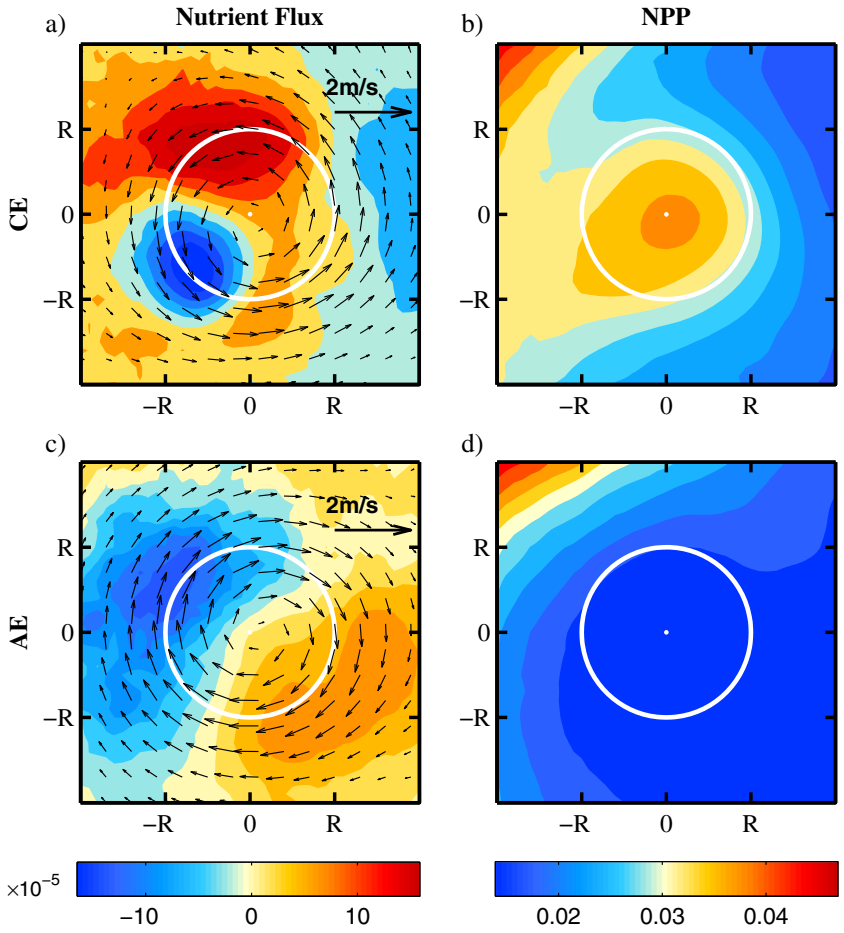

Fig. 13 Composite averages of (*first column*) nutrient flux in 100 m (in color) with horizontal current averaged in upper 50 m (in *arrows*) and (*second column*) net primary production for (*first row*) cyclonic and (*second row*) anticyclonic eddies. The nutrient includes NO_3 and SiO_4. *White lines* are circles with distance of *R* from the center (*white point*) of each panel. Unit for nutrient flux: mmol N/m^2/s. Unit for NPP: mmol N/m^3/day

possible for the growth of diatoms in some anticyclonic eddies.

From the horizontal currents, eddy advection was found to play an important role in redistributing concentrations of nutrients, phytoplankton, and zooplankton. This is consistent with the analysis in the SCS by Liu et al. (2013) and with satellite-based global observation by Chelton et al. (2011a).

Mechanism for the vertical nutrient flux structure is still unclear. In the eddy pumping theory, isopycnal displacement that occurs at the beginning of eddy formation induces upward nutrient flux in cyclonic eddies and downward flux in anticyclonic eddies (Siegel et al. 1999). The greatest vertical nutrient flux should occur at the eddy center because isopycnal displacement is the largest at eddy center. This interpretation cannot explain the structure of vertical nutrient flux in our study. Some studies suggested that the nonlinear Ekman pumping caused by wind and current interaction can induce both upward and downward motions in mesoscale eddies (Mahadevan et al. 2008; McGillicuddy et al. 2008). Some studies also revealed that net vertical motion induced by wind/eddy interaction should be upward in anticyclonic eddies and downward in cyclonic eddies (Gaube et al. 2013). This means that the wind/eddy interaction cannot explain our vertical nutrient flux structure. Further study is needed to explore the mechanism.

Combining with previous results, the possible processes of biogeochemical cycles in mesoscale eddies can be described as follows. Strong upwelling and downwelling occur at the edge of mesoscale eddies with net upward motion in cyclonic eddies and net downward motion in anticyclonic eddies. Due to strong horizontal advection, the nutrients in the euphotic zone of mesoscale eddies will be transported and mixed to generate a homogenous distribution in space (see Fig. 8). Due to the homogenous structures of nutrients and net primary production, the distribution of phytoplankton becomes homogenous as well.

3.3 Evolution of plankton communities and detritus

According to marine ecosystem simulations (Chai et al. 2002; Dugdale et al. 2002), an iron fertilization experiment (Chai et al. 2007), and a biogeochemical cycle study (Xiu and Chai 2011), the evolution of community structure was found to be caused by the predator–prey competition. Statistical analysis based on the spatial composite averages in Section 3.2 revealed that the cyclonic eddies enhanced

nutrients in the euphotic zone and stimulated the growth of plankton. But, the evolution cannot be observed in the spatial analysis.

By analyzing the biological processes within the cyclonic eddies, we find an evolution of biology community that can be described as growth–blooming–decay process during the whole lifetime in some short-lived cyclonic eddies or during a certain fragment of lifetime in some long-lived cyclonic eddies. The fragments are extracted from these long-lived eddies to be considered as "new eddies." As a result, we find a total of 79 eddies whose lifetime ranges from 27 to 117 days with an average lifetime of 43.2 days. Using the method described in Section 2.5, the constructed SLA, nutrient, biomass of plankton, and detritus during the eddy lifetime are calculated (Fig. 14). During the growing stage, cyclonic eddies intensified with the averaged SLA decreasing from −19.8 to −22.5 cm, and during the decaying stage the averaged SLA increased with a relatively lower rate. The nutrients were found to increase and decrease during the growing and decay stages, respectively, following closely with changes of SLA. At the beginning of the growth period, S1 grew fast due to the stimulation of nutrient flux from 5.23 mmol N/m^2 to a peak of 6.40 mmol N/m^2 after 8.2 days. After that, biomass of S1 fell and reached a minimum of 4.87 mmol N/m^2 due to the food competition by S2 and the increase of grazer ZZ1. During the decay period, biomass of S1 increased slightly. This phenomenon was observed in an iron fertilization numerical experiment (Chai et al. 2007). The possible reason for the second bloom is that the growth of ZZ2 grazed on S2 and ZZ1, which reduced grazing pressure on S1 (Chai et al. 2007). After getting the second peak of about 5.08 mmol N/m^2, S1 biomass decreased until the disappearance of the eddy. ZZ1 grew with a time lag to S1 and reached the peak value of 2.60 mmol N/m^2 about 8.6 days after the first peak of S1. During the end stage of the eddy life, the biomass of ZZ1 increased slightly due to the increase of S1 during the decay process. Comparing with S1, S2 increased with a larger magnitude but grew more slowly. S2 reached the maximum value at the half-time of the eddy life but fell because of the exhaustion of nutrients and the grazing of ZZ2. Feeding mainly on S2 and ZZ1, ZZ2 grew after the increases of S2 and ZZ1, reaching the peak of 7.4 mmol N/m^2 with a time lag of 8.4 days with respect to the peak of S2. As an indicator of export, DD reached the peak of 14.4 mmol N/m^2 with a time lag of 10 days with respect to the first peak of S1, and DDSi reached the peak of 12.7 mmol N/m^2 5.2 days after S2 reached its maximum value.

Now, we analyze the evolution of plankton community in the cyclonic eddies. During the eddy's lifetime, the phytoplankton bloomed due to the stimulation of nutrients and zooplankton grew because of increasing food supply. This is consistent with the spatial analysis in Section 3.2 and with the model simulation by Xiu and Chai (2011) and observational study by Chen et al. (2007) using cruise data. The results show

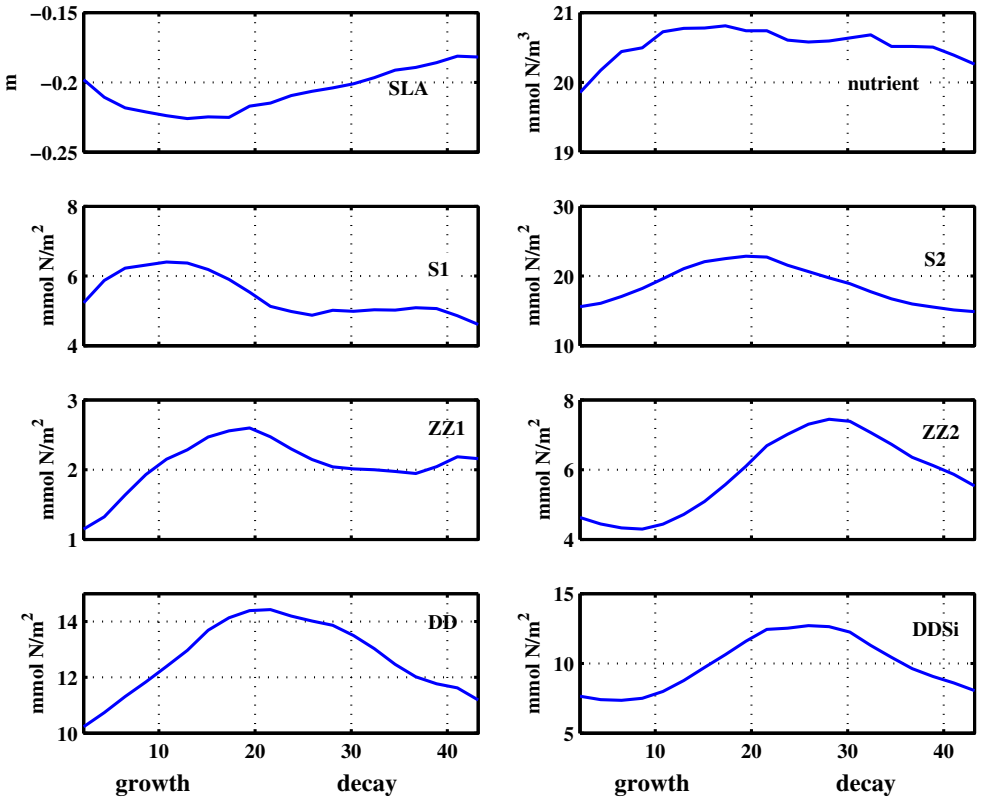

Fig. 14 Time series of SLA, nutrient, and biomass of S1, S2, ZZ1, ZZ2, DD, and DDSi constructed from 79 cyclonic eddies. (Unit in *x*-axis: day)

that both phytoplankton and zooplankton were regulated by the predator–prey relationship and followed a grow–decay period during their lifetimes. This kind of regulation of community evolution by the predator–prey relationship has been simulated in models (Chai et al. 2002; Dugdale et al. 2002). The community structure change during the eddy lifetime is consistent with the iron fertilization experiment conducted in equatorial Pacific (see Fig. 5 in Chai et al. 2007), but with larger time lags of ZZ2 with respect to S2 and of ZZ1 with respect to S1.

4 Conclusions and discussions

This study utilized a composite method to statistically analyze the mean characteristics of biogeochemical cycles associated with mesoscale eddies in the SCS. The analysis was based on the output from a three-dimensional physical–biogeochemical model simulation over 18 years and on satellite data over 10 years. A total of 568 and 315 eddies were tracked from the model and satellite SLA fields, respectively.

Our analysis about sea surface CHL for eddies revealed that cyclonic eddies were associated with high CHL and that anticyclonic eddies were associated with low CHL in the SCS. The subsequent analysis of biogeochemical variables showed that cyclonic eddies were mainly associated with abundance of nutrients, phytoplankton, and zooplankton while the anticyclonic eddies were associated with insufficient nutrients and with suppressed plankton concentrations. These results demonstrate that biogeochemical cycles associated with mesoscale eddies in the SCS are mainly controlled by eddy pumping mechanism, especially at the eddy core. Within most cyclonic eddies, the eddy pumping process induces upward nutrient flux and plankton blooms. And, within anticyclonic eddies, the eddy pumping process induces downward nutrient flux and suppresses the growth of phytoplankton and zooplankton.

From the composite results, high CHL at the west edge of the cyclonic eddies showed downstream eddy advection of CHL. Nutrients and biomasses of phytoplankton and zooplankton were distributed by anticlockwise rotational velocities in the cyclonic eddies and clockwise rotational velocities in the anticyclonic eddies. These results demonstrate that eddy advection of biogeochemical variables is probably another important physical process that influences biogeochemical cycles associated with the edge of mesoscale eddies in the SCS.

Previous studies in the Sargasso Sea and Southern Indian Ocean suggested that eddy-induced Ekman pumping considering wind–current interaction was capable of enhancing phytoplankton blooms in anticyclonic eddy cores and depressing the growth of phytoplankton inside cyclonic eddy cores (e.g., McGillicuddy et al. 2007; McGillicuddy et al. 2008; Gaube et al. 2013). Since our composite results showed that cyclonic (anticyclonic) eddy cores were mainly associated with high (low) concentration of biological variables, eddy-induced Ekman pumping mechanism is only a minor controlling process in the SCS. A more relevant case study on an anticyclonic eddy in the SCS suggested that dramatic vertical fluctuation existed when wind–current interaction was strong (Zhang et al., 2015). Two processes were discussed in Zhang et al. (2015). The first one is in horizontal direction where the imbalance of radial momentum in anticyclonic eddies can force particles to move outward and aggregate at the eddy edge. The imbalance occurs only when Rossby number is larger than 0.25, which depends on the eddy's rotation. The particles will be stable if the Rossby number is smaller than 0.25. The second process discussed in Zhang et al. (2015) is the vertical fluctuations in anticyclonic eddies triggered by eddy-induced Ekman pumping and maintained by pressure and density anomalies, as they observed isopycnals moving up and down inside anticyclonic eddies. Their results imply that anticyclonic eddies with eddy-induced Ekman pumping may also show low phytoplankton biomass at the core and high values at the edge, which is similar to the eddy pumping. But, note that their study was based on one observational case and they did not include actual biogeochemical dynamics in their analysis. Our composite results represent the general biogeochemical cycles averaged over all the anticyclonic eddies spanning a dynamic range of Rossby number. Moreover, strong eddy-induced Ekman pumping from their calculations which is almost half of the upwelling velocity observed by Argo only lasts a few days, much shorter compared with the eddy's lifespan that we are considering in this study. On the other hand, if their proposed radial imbalance and eddy-induced Ekman pumping were the dominant processes, we probably expect to see evenly distributed high concentrations of plankton and nutrients at the eddy edge surrounding the core area, which is not the case in our composite results. Therefore, we think that low concentrations of plankton and nutrients in the core of anticyclonic eddy are largely related to the eddy pumping mechanism.

In both cyclonic and anticyclonic eddies, vertical nutrient fluxes were found to have a dipole structure in the composite results. Strong upwelling and downwelling occur at the edge of eddies, with net upward motion in cyclonic eddies and net downward motion in anticyclonic eddies. As discussed before, both the eddy pumping and eddy-induced Ekman pumping theories appear to be inconsistent with the dipole structure of vertical flux. Some studies suggested that eddy-induced Ekman pumping caused by wind and current interaction can induce both upward and downward motions in mesoscale eddies (Mahadevan et al. 2008; McGillicuddy et al. 2008), and the net vertical motion induced by wind–eddy interaction should be upward in anticyclonic eddies and downward in cyclonic eddies (Gaube et al. 2013), which contradicts to the directions of net vertical flux in our study. According to the eddy pumping theory, isopycnal

displacement that occurs during the growing stage induces upward nutrient flux in cyclonic eddies and downward flux in anticyclonic eddies (Siegel et al. 1999). During the decaying stage, there are downward nutrient flux in cyclonic eddies and upward flux in anticyclonic eddies. Although the directions of net vertical flux are consistent, the greatest vertical nutrient flux induced by the eddy pumping mechanism normally occurs at the eddy center for instantaneous observation because isopycnal displacement is the largest at eddy center. It seems to contradict to the dipole structure of vertical flux as well. One possible reason for this contradiction to the eddy pumping mechanism is that our composite analysis averages all mesoscale eddies including eddy growing and decaying stages, which probably smooths the response signal at the eddy core leading to the dipole structure showing up at the eddy edge that could be caused by nonlinear Ekman or submesoscale processes. Further study is needed to explore the dynamic controlling mechanism.

The time evolution of plankton community was analyzed based on 79 long-lived cyclonic eddies. We found the decoupling evolutions of physical (e.g., SLA), biological (e.g., phytoplankton), and chemical (e.g., nutrients) structures inside mesoscale eddies (Fig. 14). Most of the previous studies were derived from instantaneous measurements that cannot cover the whole eddy evolution process, which often leads to the simple conclusion that strong cyclonic eddies can induce high nutrients, more phytoplankton, and more particles. However, our results indicate that this is not always true during the eddy's lifespan with different temporal evolution curves of different variables. For example, phytoplankton and zooplankton in eddies depend not only on the physical and chemical processes but also on the predator–prey relationships among different species of the communities. Pico-phytoplankton grew first and experienced two blooms. Micro-zooplankton, which depended on pico-phytoplankton, grew with a time lag to pico-phytoplankton. Diatoms grew in a larger magnitude than pico-phytoplankton and reached their peak value in the half-time of the eddy life. Meso-zooplankton grew after the increases of diatoms and micro-zooplankton.

Our study exhibited the general biogeochemical cycles of mesoscale eddies averaged in the SCS spatially and temporally. Further studies are needed to explore mechanisms for vertical motions at the eddy center and edge.

Acknowledgments The authors gratefully acknowledge Feng Zhou and Lili Zeng for discussion of data analysis. This research was supported by the Natural Science Foundation of Guangdong Province, China (Grant No. 2014A030306049), the CAS/SAFEA International Partnership Program for Creative Research Teams, the 100 Talent Program of Chinese Academy of Sciences, the Marine Public Welfare Research Project (Grant No. 201305019), and the China Scholarship Council (Grant No. 201306380026).

References

Basdevant C, Philipovitch T (1994) On the validity of the "Weiss criterion" in two-dimensional turbulence. Physica D: Nonlinear Phenomena 73:17–30, http://dx.doi.org/10.1016/0167-2789(94)90222-4

Bibby TS, Moore CM (2010) Silicate:nitrate ratios of upwelled waters control the phytoplankton community sustained by mesoscale eddies in sub-tropical North Atlantic and Pacific. Biogeosciences Discuss 7:7505–7525. doi:10.5194/bgd-7-7505-2010

Chai F, Dugdale RC, Peng TH, Wilkerson FP, Barber RT (2002) Wilkerson FP, Barber RT (2002) One-dimensional ecosystem model of the equatorial Pacific upwelling system. Part I: model development and silicon and nitrogen cycle. Deep Sea Res Part II: Topical Stud Oceanography 49:2713–2745, http://dx.doi.org/10.1016/S0967-0645(02)00055-3

Chai F, Jiang MS, Chao Y, Dugdale RC, Chavez F, Barber RT (2007) Modeling responses of diatom productivity and biogenic silica export to iron enrichment in the equatorial Pacific Ocean Global Biogeochemical Cycles 21:n/a-n/a doi:10.1029/2006gb002804

Chai F et al (2009) Seasonal and interannual variability of carbon cycle in South China Sea: a three-dimensional physical-biogeochemical modeling study. J Oceanogr 65:703–720. doi:10.1007/s10872-009-0061-5

Chavez FP et al (1991) Growth rates, grazing, sinking and iron limitation of equatorial Pacific phytoplankton. Limnol Oceanogr 36:1816–1833, citeulike-article-id:906409

Chelton DB, Gaube P, Schlax MG, Early JJ, Samelson RM (2011a) The influence of nonlinear mesoscale eddies on near-surface oceanic chlorophyll. Science 334:328–332. doi:10.1126/science.1208897

Chelton DB, Schlax MG, Samelson RM (2011b) Global observations of nonlinear mesoscale eddies. Prog Oceanogr 91:167–216. doi:10.1016/j.pocean.2011.01.002

Chen G, Hou Y, Chu X (2011) Mesoscale eddies in the South China Sea: mean properties, spatiotemporal variability, and impact on thermohaline structure. J Geophysical Res: Oceans 116:C06018. doi:10.1029/2010JC006716

Chen G, Hou Y, Zhang Q, Chu X (2010) The eddy pair off eastern Vietnam: interannual variability and impact on thermohaline structure. Cont Shelf Res 30:715–723, http://dx.doi.org/10.1016/j.csr.2009.11.013

Chen G, Xiu P, Chai F (2014) Physical and biological controls on the summer chlorophyll bloom to the east of Vietnam. J Oceanogr 70:323–328. doi:10.1007/s10872-014-0232-x

Chen Y-L, Chen H-Y, Lin II, Lee M-A, Chang J (2007) Effects of cold eddy on phytoplankton production and assemblages in Luzon strait bordering the South China Sea. J Oceanogr 63:671–683. doi:10.1007/s10872-007-0059-9

Coale KH et al (1996) A massive phytoplankton bloom induced by an ecosystem-scale iron fertilization experiment in the equatorial. Pacific Ocean Nature 383:495–501

Doney SC, Glover DM, McCue SJ, Fuentes M (2003) Mesoscale variability of Sea-viewing Wide Field-of-view Sensor (SeaWiFS) satellite ocean color: global patterns and spatial scales. J Geophysical Res: Oceans 108:3024. doi:10.1029/2001JC000843

Dong C, McWilliams JC, Liu Y, Chen D (2014) Global heat and salt transports by eddy movement. Nat Commun 5:3294. doi:10.1038/ncomms4294

Dugdale RC, Barber RT, Chai F, Peng TH, Wilkerson FP (2002) One-dimensional ecosystem model of the equatorial Pacific upwelling system. Part II: sensitivity analysis and comparison with JGOFS EqPac data. Deep Sea Res Part II: Topical Stud Oceanography 49:2747–2768, http://dx.doi.org/10.1016/S0967-0645(02)00056-5

Frenger I, Gruber N, Knutti R, Münnich M (2013) Imprint of southern ocean eddies on winds, clouds and rainfall. Nat Geosci 6:608–612. doi:10.1038/ngeo1863

Fujii M, Chai F, Shi L, Inoue H, Ishii M (2009) Seasonal and interannual variability of oceanic carbon cycling in the western and central tropical-subtropical pacific: a physical-biogeochemical modeling study. J Oceanogr 65:689–701. doi:10.1007/s10872-009-0060-6

Gan J, Qu T (2008) Coastal jet separation and associated flow variability in the southwest South China Sea Deep Sea Research Part I. Oceanographic Res Papers 55:1–19, http://dx.doi.org/10.1016/j.dsr.2007.09.008

Gaube P, Chelton DB, Strutton PG, Behrenfeld MJ (2013) Satellite observations of chlorophyll, phytoplankton biomass, and Ekman pumping in nonlinear mesoscale eddies. J Geophysical Res: Oceans 118:6349–6370. doi:10.1002/2013JC009027

Guo L, Chai F, Xiu P, Xue H, Rao S, Liu Y, Chavez FP (2014) Seasonal dynamics of physical and biological processes in the central California Current System: a modeling study. Ocean Dyn doi:10.1007/s10236-014-0721-x

Huang B, Hu J, Xu H, Cao Z, Wang D (2010) Phytoplankton community at warm eddies in the northern South China Sea in winter 2003/2004. Deep Sea Res Part II: Topical Stud Oceanography 57:1792–1798. doi:10.1016/j.dsr2.2010.04.005

Hwang C, Chen S-A (2000) Circulations and eddies over the South China Sea derived from TOPEX/Poseidon altimetry. J Geophysical Res: Oceans 105:23943–23965. doi:10.1029/2000JC900092

Jayne SR, Marotzke J (2002) The oceanic eddy heat transport*. J Phys Oceanogr 32:3328–3345. doi:10.1175/1520-0485(2002)032<3328:TOEHT>2.0.CO;2

Jia Y, Liu Q (2004) Eddy shedding from the Kuroshio Bend at Luzon Strait. J Oceanogr 60:1063–1069. doi:10.1007/s10872-005-0014-6

Kalnay E et al (1996) The NCEP/NCAR 40-Year Reanalysis Project. Bull Am Meteorol Soc 77:437–471. doi:10.1175/1520-0477(1996)077<0437:TNYRP>2.0.CO;2

Lévy M, Ferrari R, Franks PJS, Martin AP, Rivière P (2012) Bringing physics to life at the submesoscale. Geophys Res Lett 39, L14602. doi:10.1029/2012GL052756

Li J, Qi Y, Jing Z, Wang J (2014) Enhancement of eddy-Ekman pumping inside anticyclonic eddies with wind-parallel extension: Satellite observations and numerical studies in the South China Sea. J Mar Syst 132:150–161. doi:10.1016/j.jmarsys.2014.02.002

Lima ID, Olson DB, Doney SC (2002) Biological response to frontal dynamics and mesoscale variability in oligotrophic environments: biological production and community structure. Journal of Geophysical Research: Oceans 107:25-21-25-21 doi:10.1029/2000JC000393.

Liu F, Tang S, Chen C (2013) Impact of nonlinear mesoscale eddy on phytoplankton distribution in the northern South China Sea. J Mar Syst 123–124:33–40. doi:10.1016/j.jmarsys.2013.04.005

Liu G, Chai F (2009) Seasonal and interannual variability of primary and export production in the South China Sea: a three-dimensional physical–biogeochemical model study. ICES J Mar Sci: J du Conseil 66:420–431. doi:10.1093/icesjms/fsn219

Liu KK, Chao SY, Shaw PT, Gong GC, Chen CC, Tang TY (2002) Monsoon-forced chlorophyll distribution and primary production in the South China Sea: observations and a numerical study. Deep Sea Res Part I: Oceanographic Res Papers 49:1387–1412, http://dx.doi.org/10.1016/S0967-0637(02)00035-3

Ma W, Chai F, Xiu P, Xue H, Tian J (2013) Modeling the long-term variability of phytoplankton functional groups and primary productivity in the South China Sea. J Oceanogr 69:527–544. doi:10.1007/s10872-013-0190-8

Mahadevan A, Thomas LN, Tandon A (2008) Comment on "eddy/wind interactions stimulate extraordinary mid-ocean plankton blooms". Science 320:448. doi:10.1126/science.1152111

Martin AP, Richards KJ (2001) Mechanisms for vertical nutrient transport within a North Atlantic mesoscale eddy. Deep Sea Res Part II: Topical Stud Oceanography 48:757–773, http://dx.doi.org/10.1016/S0967-0645(00)00096-5

McGillicuddy DJ et al (2007) Eddy/wind interactions stimulate extraordinary mid-ocean plankton blooms. Science 316:1021–1026. doi:10.1126/science.1136256

McGillicuddy DJ, Johnson R, Siegel DA, Michaels AF, Bates NR, Knap AH (1999) Mesoscale variations of biogeochemical properties in the Sargasso Sea. J Geophys Res 104:13381. doi:10.1029/1999jc900021

McGillicuddy DJ, Ledwell JR, Anderson LA (2008) Response to comment on "eddy/wind interactions stimulate extraordinary mid-ocean plankton blooms". Science 320:448. doi:10.1126/science.1148974

McGillicuddy DJ et al (1998) Influence of mesoscale eddies on new production in the Sargasso Sea. Nature 394:263–266

Nan F, Xue H, Xiu P, Chai F, Shi M, Guo P (2011) Oceanic eddy formation and propagation southwest of Taiwan. J Geophysical Res: Oceans 116:C12045. doi:10.1029/2011JC007386

Ning X, Peng X, Le F, Hao Q, Sun J, Liu C, Cai Y (2008) Nutrient limitation of phytoplankton in anticyclonic eddies of the northern South China Sea. Biogeosciences Discuss 5:4591–4619. doi:10.5194/bgd-5-4591-2008

Okubo A (1970) Horizontal dispersion of floatable particles in the vicinity of velocity singularities such as convergences. Deep Sea Res Oceanographic Abstracts 17:445–454, http://dx.doi.org/10.1016/0011-7471(70)90059-8

Qiu B, Chen S (2005) Eddy-induced heat transport in the subtropical North Pacific from Argo, TMI, and altimetry measurements. J Phys Oceanogr 35:458–473. doi:10.1175/JPO2696.1

Shchepetkin AF, McWilliams JC (2003) A method for computing horizontal pressure-gradient force in an oceanic model with a nonaligned vertical coordinate. J Geophysical Res: Oceans 108:3090. doi:10.1029/2001JC001047

Shchepetkin AF, McWilliams JC (2005) The regional oceanic modeling system (ROMS): a split-explicit, free-surface, topography-following-coordinate oceanic model. Ocean Model 9:347–404. doi:10.1016/j.ocemod.2004.08.002

Siegel DA, Court DB, Menzies DW, Peterson P, Maritorena S, Nelson NB (2008) Satellite and in situ observations of the bio-optical signatures of two mesoscale eddies in the Sargasso Sea. Deep Sea Res Part II: Topical Stud Oceanography 55:1218–1230, http://dx.doi.org/10.1016/j.dsr2.2008.01.012

Siegel DA, McGillicuddy DJ, Fields EA (1999) Mesoscale eddies, satellite altimetry, and new production in the Sargasso Sea. J Geophysical Res: Oceans 104:13359–13379. doi:10.1029/1999JC900051

Siegel DA, Peterson P, McGillicuddy DJ, Maritorena S, Nelson NB (2011) Bio-optical footprints created by mesoscale eddies in the Sargasso Sea. Geophysical Research Letters 38:n/a-n/a doi:10.1029/2011gl047660

Song Y, Haidvogel D (1994) A semi-implicit ocean circulation model using a generalized topography-following coordinate system. J Comput Phys 115:228–244, http://dx.doi.org/10.1006/jcph.1994.1189

Thomas LN, Tandon A, Mahadevan A (2013) Submesoscale processes and dynamics. In: Ocean Modeling in an Eddying Regime. American Geophysical Union, pp 17–38. doi:10.1029/177GM04

Volkov DL, Lee T, Fu L-L (2008) Eddy-induced meridional heat transport in the ocean. Geophys Res Lett 35, L20601. doi:10.1029/2008GL035490

Wang G, Su J, Chu PC (2003) Mesoscale eddies in the South China Sea observed with altimeter data. Geophys Res Lett 30:2121. doi:10.1029/2003GL018532

Wang J, Tang D, Sui Y (2010) Winter phytoplankton bloom induced by subsurface upwelling and mixed layer entrainment southwest of Luzon Strait. J Mar Syst 83:141–149, http://dx.doi.org/10.1016/j.jmarsys.2010.05.006

Weiss J (1991) The dynamics of enstrophy transfer in two-dimensional hydrodynamics. Physica D: Nonlinear Phenomena 48:273–294, http://dx.doi.org/10.1016/0167-2789(91)90088-Q

Xiu P, Chai F (2011) Modeled biogeochemical responses to mesoscale eddies in the South China Sea. J Geophysical Res: Oceans 116: C10006. doi:10.1029/2010JC006800

Xiu P, Chai F, Shi L, Xue H, Chao Y (2010) A census of eddy activities in the South China Sea during 1993–2007. J Geophysical Res: Oceans 115:C03012. doi:10.1029/2009JC005657

Xiu P, Chai F, Xue H, Shi L, Chao Y (2012) Modeling the mesoscale eddy field in the Gulf of Alaska. Deep Sea Res Part I: Oceanographic Res Papers 63:102–117. doi:10.1016/j.dsr.2012.01.006

Yang H, Liu Q (2003) Forced Rossby wave in the northern South China Sea. Deep Sea Res Part I: Oceanographic Res Papers 50:917–926. doi:10.1016/S0967-0637(03)00074-8

Yuan D, Han W, Hu D (2007) Anti-cyclonic eddies northwest of Luzon in summer-fall observed by satellite altimeters Geophysical Research Letters 34:n/a-n/a doi:10.1029/2007gl029401

Zhang H-M, Bates JJ, Reynolds RW (2006) Assessment of composite global sampling: sea surface wind speed Geophysical Research Letters 33 doi:10.1029/2006gl027086

Zhang Z, Wang W, Qiu B (2014) Oceanic mass transport by mesoscale eddies. Science 345:322–324. doi:10.1126/science.1252418

Zhao H, Tang DL (2007) Effect of 1998 El Niño on the distribution of phytoplankton in the South China Sea. J Geophysical Res: Oceans 112:C02017. doi:10.1029/2006JC003536

Zhong Y, Bracco A (2013) Submesoscale impacts on horizontal and vertical transport in the Gulf of Mexico. J Geophysical Res: Oceans 118:5651–5668. doi:10.1002/jgrc.20402

Zhou K et al (2013) Apparent enhancement of 234Th-based particle export associated with anticyclonic eddies. Earth Planet Sci Lett 381:198–209. doi:10.1016/j.epsl.2013.07.039

Zhang W-Z, Xue H, Chai F, Ni Q (2015) Dynamical processes within an anticyclonic eddy revealed from Argo floats. Geophys Res Lett 42: 2342–2350. doi:10.1002/2015gl063120